

Layer-by-Layer Assembled Gold Nanoshells for the Intracellular Delivery of miR-34a

RITU GOYAL,¹ CHINTAN H. KAPADIA,¹ JILIAN R. MELAMED,¹ RACHEL S. RILEY,¹ and EMILY S. DAY ^{1,2,3}

¹Department of Biomedical Engineering, University of Delaware, 161 Colburn Lab, Newark, DE 19716, USA; ²Department of Materials Science & Engineering, University of Delaware, Newark, DE, USA; and ³Helen F. Graham Cancer Center & Research Institute, Newark, DE, USA

(Received 15 February 2018; accepted 26 May 2018)

Associate Editor Lola Eniola-Adefeso oversaw the review of this article.

Abstract

Introduction—MicroRNAs (miRNAs) are short noncoding RNAs whose ability to regulate the expression of multiple genes makes them potentially exciting tools to treat disease. Unfortunately, miRNAs cannot passively enter cells due to their hydrophilicity and negative charge. Here, we report the development of layer-by-layer assembled nanoshells (LbL-NS) as vehicles for efficient intracellular miRNA delivery. Specifically, we developed LbL-NS to deliver the tumor suppressor miR-34a into triple-negative breast cancer (TNBC) cells, and demonstrate that these constructs can safely and effectively regulate the expression of SIRT1 and Bcl-2, two known targets of miR-34a, to decrease cell proliferation.

Methods—LbL-NS were made by coating negatively charged nanoshells with alternating layers of positive poly-L-lysine (PLL) and negative miRNA, with the outer layer consisting of PLL to facilitate cellular entry and protect the miRNA. Electron microscopy, spectrophotometry, dynamic light scattering, and miRNA release studies were used to characterize LbL-NS. The particles' ability to enter MDA-MB-231 TNBC cells, inhibit SIRT1 and Bcl-2 expression, and thereby

reduce cell proliferation was examined by confocal microscopy, Western blotting, and EdU assays, respectively.

Results—Each successive coating reversed the nanoparticles' charge and increased their hydrodynamic diameter, resulting in a final diameter of 208 ± 4 nm and a zeta potential of 53 ± 5 mV. The LbL-NS released $\sim 30\%$ of their miR-34a cargo over 5 days in $1\times$ PBS. Excitingly, LbL-NS carrying miR-34a suppressed SIRT1 and Bcl-2 by 46 ± 3 and $35 \pm 3\%$, respectively, and decreased cell proliferation by 33%. LbL-NS carrying scrambled miRNA did not yield these effects.

Conclusion—LbL-NS can efficiently deliver miR-34a to TNBC cells to suppress cancer cell growth, warranting their further investigation as tools for miRNA replacement therapy.

Keywords—MicroRNA, Nanoparticles, RNA interference, Gene regulation, Poly-L-lysine, Trafficking, Release, SIRT1, Bcl-2, Triple-negative breast cancer.

Address correspondence to Emily S. Day, Department of Biomedical Engineering, University of Delaware, 161 Colburn Lab, Newark, DE 19716, USA. Electronic mail: emilyday@udel.edu

Emily S. Day is an Assistant Professor in the Department of Biomedical Engineering at the University of Delaware. Dr. Day completed her Ph.D. at Rice University in 2006, where she trained with Dr. Jennifer West. There, her research focused on developing nanoparticle-mediated photothermal therapy for treatment of glioblastoma, an aggressive form of primary brain tumor. While at Rice, Dr. Day received a National Science Foundation Graduate Research Fellowship, a Rice President's Graduate Fellowship, and a Howard Hughes Medical Institute Med-Into-Grad Fellowship. Upon completing her Ph.D., Dr. Day joined the laboratory of Dr. Chad Mirkin at Northwestern University, where she developed RNA-nanoparticle conjugates known as spherical nucleic acids for gene regulation of glioblastoma. Dr. Day was awarded an International Institute for Nanotechnology Postdoctoral Fellowship and a National Institutes of Health F32 Ruth L. Kirschstein National Research Service Award during her time at Northwestern University. Dr. Day started her lab at the University of Delaware in 2013, and her group investigates the interactions between nanoparticles and biological systems to create novel engineering tools for high precision

cancer therapy. She has received numerous grants to support her work, including a W.M. Keck Foundation Grant, an NIH/NIGMS R35 Outstanding Investigator Award, and an NSF CAREER.

This article is part of the 2018 CMBE Young Innovators special issue.



ABBREVIATIONS

DEPC	Diethyl pyrocarbonate
DLS	Dynamic light scattering
DMEM	Dulbecco's Modified Eagle Medium
DMF	Dimethylformamide
DNA	Deoxyribonucleic acid
EdU	5-Ethynyl-2'-deoxyuridine
FBS	Fetal bovine serum
LAMP-1	Lysosomal-associated membrane protein 1
LbL	Layer-by-layer
LbL-NS	Layer-by-layer assembled nanoshells
MCC	Mander's colocalization coefficient
mRNA	Messenger RNA
miRNA	microRNA
MUA	11-Mercaptoundecanoic acid
NaCl	Sodium chloride
NaOH	Sodium hydroxide
NS	Nanoshells
OD	Optical density
PLL	Poly-L-lysine
RIPA	Radioimmunoprecipitation assay
RNA	Ribonucleic acid
RNAi	RNA interference
RPM	Rotations per minute
SEM	Scanning electron microscopy
SNAr	Nucleophilic aromatic substitution reaction
TNBC	Triple-negative breast cancer
TNBS	2,4,6-Trinitrobenzenesulfonic acid
TNP	Trinitrophenyl
TRITC	Tetramethylrhodamine isothiocyanate
UV-Vis	Ultra violet-visible spectrophotometry

INTRODUCTION

MicroRNA (miRNA) molecules are small, evolutionary conserved, noncoding ribonucleic acids that account for 1–5% of the total human genome.²⁶ Although the specific biological functions of miRNAs are not fully understood, miRNAs are known to regulate gene expression to control cellular and metabolic pathways, and miRNAs have been reported to regulate at least 30% of protein-coding genes.^{4,7,26} miRNAs regulate gene expression by binding targeted messenger RNA (mRNA) molecules with either perfect or imperfect complementarity to trigger mRNA degradation or translational repression.¹⁸ The ability of miRNAs to regulate the expression of multiple genes through RNA interference (RNAi) has created intense interest in their use as tools to halt disease progression, particularly in diseases where endogenous expression

of an inhibitory miRNA is low. For example, among over 700 identified miRNAs in human cells, miRNA-34a (miR-34a) has become one of the most well studied tumor suppressors.^{1,33,34} Research has shown that miR-34a inhibits several mRNAs associated with tumor growth, including SIRT1 and Bcl-2 (which are known to inhibit apoptosis and repress cell cycle arrest), and its loss of expression is common in many cancers and associated with a poor prognosis.^{24,29,33,40} Accordingly, miR-34a is an attractive molecule for miRNA replacement therapy. However, its intracellular delivery remains a challenge. In this study, we aimed to develop a new nanocarrier platform to facilitate miR-34a delivery into triple-negative breast cancer (TNBC) cells.

Triple-negative breast cancer (TNBC) accounts for 15–25% of breast cancers, and has earlier relapse and higher mortality rates than other breast cancer subtypes because of its aggressive behavior.^{22,25} The expression of miR-34a is lost in TNBC, and this loss-of-expression leads to more aggressive tumor cell behavior.^{3,24} It has been shown that restoring miR-34a expression in TNBC cells can inhibit cell proliferation and invasion, activate senescence, and promote drug sensitivity.^{2,8,21,23} Unfortunately, like other miRNAs, the successful delivery of miR-34a into TNBC cells remains a challenge to its clinical translation. Naked miRNA molecules cannot passively cross negatively charged cell membranes because of their large size and negative charge.⁶ To overcome this issue, researchers have employed polycationic materials as agents to condense and protect nucleic acids and shuttle them into cells.^{6,20} Among the various polycationic materials investigated for nucleic acid delivery, poly-L-lysine (PLL) has shown promise as it binds well with the negative backbone of nucleic acids, and it provides enough buffering capacity to release nucleic acid cargo from endocytic vesicles inside cells.³⁹ However, PLL is inherently toxic due to the presence of primary amines on its backbone,³⁵ and simple PLL-nucleic acid polyplexes do not allow fine control over parameters that are critical for miRNA delivery, such as the relative ratio of polycation to miRNA or the overall size of the construct. Layer-by-layer (LbL) nanoparticles that are made by sequential deposition of oppositely charged polymers around a spherical nanoparticle core offer an exciting strategy to fine-tune nanoscale architecture and improve miRNA delivery.^{9,11,16,31} Here, we employ the LbL deposition approach to coat silica core/gold shell nanoshells (NS) with alternating layers of PLL and miR-34a. NS possess several advantages as a core carrier platform, including ease of synthesis that results in a narrow size distribution, simple surface modification, and validated safety in human clinical trials.³⁶

In this study, we aimed to deliver miR-34a to MDA-MB-231 TNBC cells using layer-by-layer assembled nanoshells (LbL-NS). We hypothesized that the layered structure would efficiently load miR-34a, and that the LbL-NS would enter cells by endocytosis due to the positive charge of the outermost layer of PLL. We also hypothesized that miR-34a would be released from LbL-NS in the physiological environment. To test these hypotheses, we synthesized LbL-NS and characterized them with dynamic light scattering, scanning electron microscopy, and spectrophotometry measurements. We also analyzed RNA loading and release. Further, confocal microscopy was used to assess LbL-NS trafficking in cells, which demonstrated the nanoparticles are taken up by endocytosis and follow a similar trafficking pattern to PLL-miRNA polyplexes. To confirm the functionality of the delivered miR-34a, we analyzed treated cells for expression of SIRT1 and Bcl-2 *via* Western blotting, and we measured cellular proliferation by EdU assays. Together, our data show that LbL-NS are potent and safe vehicles for intracellular miR-34a delivery that are more effective than PLL-miR-34a polyplexes. The observation that LbL-NS with precisely defined architecture are more effective than randomly assembled PLL-miRNA polyplexes suggests that tailoring the structure of nanoscale miRNA carriers is critical to their function. While we investigated the use of LbL-NS for delivery of miR-34a into TNBC cells in this work, our findings suggest that LbL-NS may be a great platform for the delivery of other miRNA molecules to various cell types. Further studies are warranted to more broadly explore and optimize these LbL-NS as tools for application in miRNA replacement therapy.

MATERIALS AND METHODS

Synthesis of Layer-by-Layer Assembled Nanoshells (LbL-NS)

Nanoshells comprised of 120 nm diameter silica cores and 15 nm thick gold shells were synthesized using a previously published protocol.³⁰ Briefly, 2–3 nm colloidal gold was prepared by the Duff method¹⁰ and combined with 120 nm diameter 3-aminopropyltriethoxysilane-coated silica nanoparticles (Nanocomposix). The mixture rocked at room temperature for several days, after which any unreacted colloidal gold was removed by centrifugation (2800 rpm, 25 min) and removal of the supernatant. Additional gold was then reduced with formaldehyde onto the gold nucleation sites present on the silica cores to form complete gold shells. The resultant nanoshells (NS) were treated with 0.1% diethyl pyrocarbonate (DEPC) for 3 days at 37 °C to render the solution RNase-free.

To provide a more negative surface charge and to facilitate electrostatic binding with PLL, the synthesized nanoshells were coated with 11-mercaptopoundecanoic acid (MUA). To do this, the pH of the NS solution (stored at an optical density (OD) = 1, corresponding to 2.7×10^9 NS mL⁻¹) was adjusted to 11 using 1 N NaOH, and then MUA (20 mg mL⁻¹ in ethanol) was added drop wise to a final concentration of 0.1 mg mL⁻¹. All reagents used in the synthesis were purchased or treated with DEPC to be RNase-free prior to use. The MUA-coated nanoshells (NS-MUA) were shaken at room temperature for 3 days and then purified twice by centrifuging (1500×g, 7 min) to form a nanoparticle pellet and removing unbound MUA with the supernatant. After the supernatant was removed, the NS-MUA were suspended in 10 mM NaCl.

To coat the NS-MUA with PLL, the purified NS-MUA (100 mL, OD = 1) were added drop wise to PLL (5 mL, 1 mg mL⁻¹ in water) while stirring (500 rpm, room temperature). The particles (NS-MUA-PLL-1) were purified twice by centrifugation (1500×g, 7 min) and were resuspended in 10 mM RNase-free NaCl. The amount of unbound PLL in solution was quantified using a 2,4,6-trinitrobenzenesulfonic acid (TNBS) assay for detection of primary amines.¹⁵ The free acid of TNBS has a pK_a below 0. TNBS reacts with primary amines in a nucleophilic aromatic substitution reaction (S_NAr) yielding trinitrophenyl (TNP)-labeled amino groups, which can be measured by UV-Vis spectrophotometry (Cary60, Agilent) at a peak wavelength of 344 nm. Researchers have used this assay extensively for direct quantification of primary amines on polymers.^{13,37}

Next, the particles were coated with miRNA (IDT DNA) by adding either miR-34a or scrambled miRNA (miR-co) duplexes to the PLL-coated NS. In initial characterization studies miRNA was added to OD = 1 PLL-NS at a final concentration of 500 nM, and this was later reduced to 250 nM miRNA per OD = 4 PLL-NS for *in vitro* studies. The sequences used were: (i) miR-34a sense: 5'-A CAA CCA GCU AAG ACA CUG CCA-3'; (ii) miR-34a antisense: 5'-UGG CAG UGU CUU AGC UGG UUG U-3'; (iii) miR-co sense: 5'-AAG UGA UCA AGC ACC GAA GAG-3' (iv) miR-co antisense: 5'-CUC UUC GGU GCU UGA UCA CUU-3'. Note that the miR-34a antisense sequence is the mature miR-34a sequence, as opposed to the entire hairpin structure, as delivery of mature miRNA is typical for miRNA nanocarrier systems.^{17,19} After miRNA addition, the particles were shaken at room temperature for 30 min, then purified twice using centrifugation (1500×g, 7 min) to remove unbound miRNA with the supernatant before being suspended in 10 mM RNase-free NaCl. The amount of miRNA

bound to the nanoparticles was determined by quantifying the miRNA remaining in solution with a Quant-IT OliGreen assay (ThermoFisher Scientific).²⁸ Finally, the second and outer coating of PLL was added to the nanoparticles in the same manner as the first coating. The purified LbL-NS were stored in 10 mM RNase-free NaCl at 4 °C until use.

Nanoparticle Characterization

After the addition of each layer (MUA, PLL, miRNA, and PLL), the purified nanoparticles were characterized by UV-Vis spectrophotometry (Cary60, Agilent), scanning electron microscopy (SEM, Hitachi S4700), and dynamic light scattering (DLS) and/or zeta potential measurements (Litesizer500, Anton Paar). For spectrophotometry, the NS were transferred to a disposable cuvette and scanned on a spectrophotometer from 1100 to 400 nm, using a 2400 nm min⁻¹ scan speed, after subtracting the baseline with water. The OD of the NS was determined using λ_{max} and NS concentration was calculated using the peak absorbance at λ_{max} and Lambert-Beer's law.

To visualize the nanoparticles at each coating step, SEM stubs (Electron Microscopy Sciences) were coated with silicon wafers (5 × 7 mm, Ted Pella) and the NS were directly dried on these wafers after suspending and diluting them in ethanol. Each stub was sputter coated with platinum (2 nm thick, Leica EM ACE600). Imaging was performed using a Hitachi S4700 at three magnifications: 50, 80 and 100 k. The diameter of the coated NS was measured as the average of 15–30 particles using ImageJ software.

The hydrodynamic diameters of the NS (suspended in 10 mM NaCl) were measured by DLS in triplicate after each coating step using an Anton Paar LiteSizer 500. Data analysis was performed in automatic mode and measured sizes were presented as the average value of 20 runs. Zeta potential measurements of the NS (diluted in 10 mM NaCl) were also carried out after each coating step using the same LiteSizer 500 instrument with 30 runs in triplicate and the average values were estimated by using the Smoluchowski approximation.

Quantifying the Release of miR-34a from LbL-NS in Phosphate Buffered Saline

To quantify the release of miR-34a from LbL-NS, 1 mL of particles suspended in 1× phosphate buffered saline (PBS) at OD = 2, synthesized with a 250 nM starting concentration of miR-34a, was incubated at 37 °C for 2 h. After 2 h, the particles were centrifuged for 7 min at 1500×g to form a pellet and the supernatant containing released miR-34a was collected in a

separate tube for quantification by OliGreen assay. Fresh 1× PBS was added to replenish the volume and the particles were probe sonicated for ~ 5 s at low power. Similarly, the particles were further incubated at 37 °C for 4, 6, 8, 24, 48, 74, 96 and 120 h and supernatants collected at each time point and stored at 4 °C. At the conclusion of the experiment, the supernatants were analyzed using OliGreen assay to quantify the amount of miR-34a released in solution. The amount of miRNA released was divided by the amount of miRNA initially loaded in order to calculate the percent cumulative release at each time point. The data is plotted as the mean of three independent experiments.

To assess the stability of LbL-NS under storage conditions (4 °C in 10 mM NaCl), we similarly analyzed miR-34a release by OliGreen assay at 0, 3, 8, 17, 23, 28, 31, 48, 57, and 66 days. To corroborate the OliGreen data, we measured the hydrodynamic diameter and zeta potential of the nanoparticles at each of these time points using an Anton Paar LiteSizer 500, as described above.

Preparation of MDA-MB-231.LAMP1-mGFP Cells for Nanoparticle Trafficking Studies

MDA-MB-231 TNBC cells (American Type Culture Collection) and 293TN lentiviral producer cells (System Biosciences) were cultured in Dulbecco's modified eagle medium (DMEM) (VWR) supplemented with 10% FBS (Gemini Bio-Products) and 1% penicillin/streptomycin (ThermoFisher Scientific). Cells were maintained in a humidified environment at 37 °C, 5% CO₂. To prepare a stably gene expressing cell line that would enable analysis of nanoparticle trafficking to lysosomes, MDA-MB-231 cells were stably transduced with LAMP1-mGFP using standard lentiviral procedures. Briefly, LAMP1-mGFP (Addgene #34831) was cloned into a lentiviral transfer vector (System Biosciences) by restriction enzyme digest. Lentiviral particles were produced by triple-transfecting (TransIT-Lenti transfection reagent; Mirus Bio LLC) 293TN cells with the LAMP1-mGFP transfer vector and lentiviral packaging and envelope plasmids (Addgene #12260, 12259). Lentivirus was harvested, filtered, and diluted in cell culture medium to transduce MDA-MB-231 cells. Then, 1 μg mL⁻¹ puromycin (VWR) was used to select cells stably expressing LAMP1-mGFP (MDA-MB-231.LAMP1-mGFP).

Analysis of Nanoparticle Trafficking in MDA-MB-231.LAMP-1-mGFP Cells

Confocal microscopy was used to track the intracellular delivery of LbL-NS and compare their cell

uptake and localization against PLL polyplexes. PLL was labeled with tetramethylrhodamine isothiocyanate (TRITC) using previously reported methods.¹⁴ Briefly, PLL (1.5 mL at 10 mg mL⁻¹ in DI water) was reacted by shaking with TRITC (50 μ L at 10 mg mL⁻¹ in DMF) overnight at room temperature to label 1% of the total amines. The reaction mixture was lyophilized and stored at -20 °C until use. LbL-NS were prepared as described above by replacing unmodified PLL with TRITC-PLL and miR-34a with Cy5-labeled RNA (sense: 5'-CCAGGAAUUUGACUCCCAAdTdT-3'; antisense: 5'-UUGGGAGUCAAAUCCUGGCdT-Cy5-3'). Polyplexes of PLL (1 μ g) and Cy5 RNA (250 nM) were prepared the same day of treatment and incubated for 30 min at room temperature before adding to cells. MDA-MB-231.LAMP1-mGFP cells were seeded in 35 mm glass bottom dishes at a density of 150,000 cells/dish and cultured overnight. Cells were incubated with labeled PLL-RNA polyplexes (1 μ g PLL; 250 nM RNA) or LbL-NS (containing 250 nM Cy5 RNA) for 6 h at 37 °C, 5% CO₂, washed three times with PBS to remove non-internalized nanocomplexes, and replenished with fresh medium. Cells were incubated for an additional 18 h prior to imaging. Live cell confocal microscopy was performed using a Zeiss LSM880 confocal microscope equipped with an incubated stage to maintain cells, and quantitative colocalization analysis was conducted to assess the intracellular stability and localization of constructs. Briefly, z-stacks were acquired to analyze construct distribution throughout the volume of the cell. Image analysis was performed on regions of interest defined by manually tracing individual cells. The Cy5-RNA, LAMP1-mGFP, and TRITC-PLL channels were median filtered with a 3-by-3-by-3 neighborhood and top-hat filtered using a 2 μ m disk element. Manders' colocalization coefficients (MCCs) were calculated for each pair of probes in each region of interest.²⁷ The intracellular localization of LbL-NS carrying Cy5-labeled RNA was similarly assessed at 72 h by incubating MDA.MB.231-LAMP1-mGFP cells with LbL-NS for 6 h, washing thrice with PBS to remove non-internalized nanoparticles, then incubating an additional 66 h in fresh medium prior to imaging with a Zeiss LSM880 confocal microscope.

Analysis of SIRT1 and Bcl-2 by Western Blotting

MDA-MB-231 cells were cultured in 6-well plates in complete medium at a density of 100,000 cells per well and treated with miR-34a-LbL-NS, miR-co-LbL-NS, or no nanoparticles for 72 h. Cells were lysed in radioimmunoprecipitation assay (RIPA) buffer (Amresco) supplemented with Halt Protease Inhibitory Cocktail (Life Technologies) according to the manu-

facturer's protocol and the cell lysate was used to assess the expression of SIRT1 and Bcl-2, two genes that are directly regulated by miR-34a, in order to evaluate the successful intracellular delivery of miR-34a. Protein concentration was determined using a DC Protein Assay (BioRad) and 30 μ g of protein was separated on 4–12% Bis-tris gels at 135 V for 60 min. Then, the protein was transferred to 0.2 μ m nitrocellulose membranes for 10 min using the Pierce Power System (Thermo Scientific). Membranes were blocked for 60 min in 5% milk prepared in tris buffered saline with 0.1% Tween-20 (TBST) and then incubated with rabbit SIRT1 and Bcl-2 antibodies (Proteintech) diluted 1:1000 in TBST with 5% milk overnight at 4 °C. After overnight incubation, membranes were washed thrice in TBST and incubated with HRP-mouse anti-rabbit IgG (Santa Cruz) diluted 1:25,000 in TBST with 5% milk for 1 h at room temperature. Membranes were washed twice in TBST, followed by once in TBS (without Tween-20) and protein bands were visualized using an Amersham enhanced chemiluminescence detection solution (GE Healthcare). Band intensity quantification (i.e., densitometry) was performed in ImageJ using actin as the housekeeping gene to quantify the level of protein suppression for each target as the average and standard deviation across three independent experiments. The blot shown is representative of the three independent experiments performed.

Analysis of Cellular Metabolic Activity upon Treatment with LbL-NS

MDA-MB-231 cells were maintained (37 °C, 5% CO₂) in DMEM with 10% heat inactivated fetal bovine serum and 1% antibiotic cocktail of streptomycin and penicillin, as described above. Cells were cultured in 96 well plates at a density of 5000 cells per well. To reveal the inherent toxicity of PLL, the cells were treated in triplicate with free PLL (1, 5, 10, 20, 30, 40, 50, 75 or 100 μ g mL⁻¹) and incubated for 72 h before using Alamar Blue assays (Thermo Fisher Scientific) to assess cellular metabolic activity per the manufacturer's protocol. To reveal the cytocompatibility of LbL-NS and distinguish the impact that miR-34a delivered with LbL-NS has on cellular metabolic activity, MDA-MB-231 cells cultured in 96 well plates at 5000 cells per well were exposed to LbL-NS prepared with miR-co or miR-34a at concentrations ranging from OD 0.5–4. The LbL-NS used for these experiments were synthesized by adding 250 nM miRNA to OD4 PLL-coated NS, as described in the synthesis section above. After incubating 72 h, cellular metabolic activity was analyzed by Alamar Blue assay. In these experiments, untreated cells were analyzed as 100% viable. After incubating each sample with the

AlamarBlue reagent, its fluorescence was read on a Biotek Synergy H1 M plate reader. A Student's *t* test was used to determine statistical differences in metabolic activity between samples treated with miR-co-LbL-NS and miR-34a-LbL-NS at each dose.

To understand the impact of LbL-NS on non-cancerous cells, we measured the metabolic activity of MCF10A breast epithelial cells exposed to miR-co-LbL-NS or miR-34a-LbL-NS. MCF10A cells were cultured in a 50:50 DMEM and F12 base medium supplemented with 5% FBS, 10 $\mu\text{g mL}^{-1}$ insulin, 0.5 $\mu\text{g mL}^{-1}$ hydrocortisone, 50 $\mu\text{g mL}^{-1}$ bovine pituitary extract, 20 ng mL^{-1} epidermal growth factor, and 100 ng mL^{-1} cholera toxin. Cells were incubated in culture flasks at 37 °C in a 5% CO₂ environment. For analysis of metabolic activity, MCF10A cells were transferred to 96 well plates at 5000 cells per well and exposed to LbL-NS prepared with miR-co or miR-34a at a dose of OD 3 (corresponding to ~ 200 nM miRNA). After incubating 72 h, cellular metabolic activity was analyzed by Alamar Blue assay as described above with untreated cells analyzed as 100% viable.

Analysis of Cell Proliferation upon Treatment with LbL-NS

Since miR-34a is known to regulate cell proliferation, we used EdU proliferation assays to demonstrate the efficacy of LbL-NS and compare their potency to PLL-miRNA polyplexes. For this study, cells were treated with polyplexes made with 250 nM miRNA and 1 $\mu\text{g mL}^{-1}$ PLL, or with LbL-NS made with 250 nM miRNA per OD4 PLL-coated NS. MDA-MB-231 cells were seeded in 12-well culture plates at 25,000 cells per well and cultured in DMEM supplemented with 10% FBS and 1% penicillin–streptomycin overnight. The cells then incubated with miR-co-PLL polyplexes, miR-34a-PLL polyplexes, miR-co-LbL-NS, or miR-34a-LbL-NS diluted in complete culture medium for 6 h. Non-internalized constructs were removed by washing thrice with 500 μL PBS and the cells were further incubated for 48 h. A Click-IT EdU assay kit (ThermoFisher Scientific) was used to measure cell proliferation according to the manufacturer's protocol. Briefly, EdU (0.5 μL per well) was added to the cells and incubated for 16–20 h at 37 °C, 5% CO₂. Cells were trypsinized, fixed, and EdU detected with AlexaFluor488-azide using copper-catalyzed click reaction per the manufacturer's protocol, and suspended in 1 \times PBS for determination of cellular proliferation by flow cytometry using a NovoCyte flow cytometer (ACEA Biosciences). AlexaFluor488 was detected using 488 nm excitation coupled to a 530/

30 nm detector. Statistical differences between groups were determined by analysis of variance.

To evaluate the impact of LbL-NS on proliferation of non-cancerous cells, MCF10A cells were cultured as described above and exposed to no treatment, miR-co-PLL polyplexes, miR-34a-PLL polyplexes, miR-co-LbL-NS, or miR-34a-LbL-NS diluted in complete culture medium at a dose corresponding to 250 nM miRNA for 6 h. Non-internalized constructs were removed by washing thrice with PBS and the cells incubated an additional 48 h prior to analysis of proliferation with a Click-IT EdU assay kit as described above.

RESULTS AND DISCUSSION

Layer-by-Layer Nanoshell (LbL-NS) Synthesis and Characterization

Nanoshells were synthesized using a previously published protocol³⁰ and coated step-wise with (i) MUA, (ii) PLL, (iii) miR-34a or miR-co, and (iv) PLL (Fig. 1a). At each step, UV–Vis spectrophotometry, SEM, DLS, and zeta potential measurements were used to characterize the particles, and the amounts of PLL and miR-34a loaded onto the nanoparticles were quantified by TNBS and OliGreen assays, respectively. The UV–Vis spectrophotometry data showed that uncoated NS had peak extinction around 800 nm, which red-shifted by a few nanometers after the addition of each layer (Fig. 1b). This minor red-shift in the plasmon peak after each coating suggests that the particles were successfully coated and maintained their structure and morphology during the coating procedure (Fig. 1b). DLS showed that the particles' hydrodynamic diameter increased by ~ 5 nm after the addition of each MUA or PLL layer, and increased by ~ 25 nm when the miRNA layer was added (Fig. 1c), such that the final diameter of miR-34a-LbL-NS was 208 \pm 4 nm. The observations from spectrophotometry and DLS were well supported by zeta potential measurements (Fig. 1d) and by SEM (Fig. 2), which showed the nanoparticles had a spherical morphology after each layer was added and their size increased approximately 5 nm per MUA or PLL layer, with a larger increase observed following addition of the miRNA layer (Fig. 2).

With respect to the zeta potential measurements (Fig. 1d), we determined that the bare NS possess a negative zeta potential (~ - 24.0 mV), which remained negative (- 29.3 mV) after coating with MUA due to the presence of negative carboxylic acid functionalities at the end. The zeta potential became positive

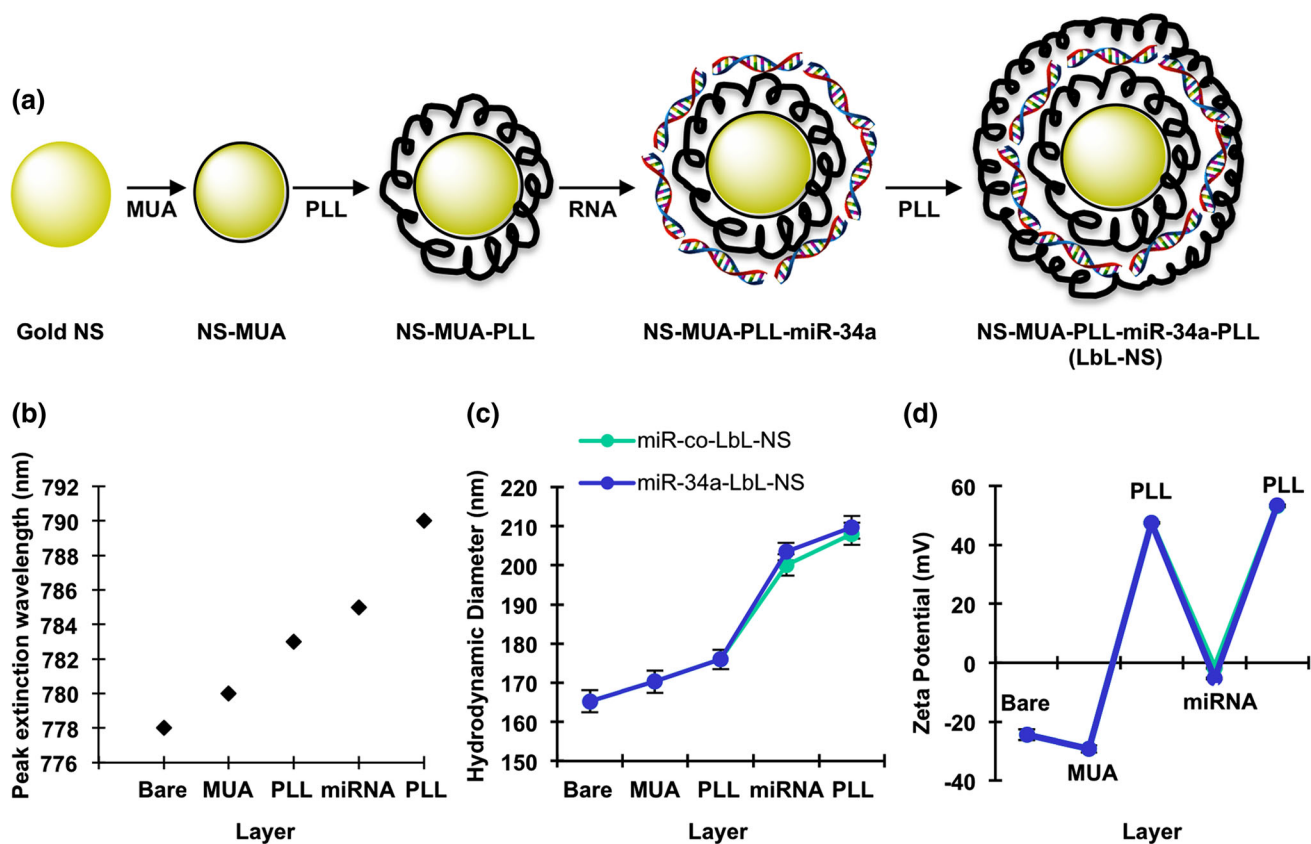


FIGURE 1. (a) Schematic of the synthesis of layer-by-layer assembled nanoshells (LbL-NS) (drawing not to scale). (b) Peak extinction wavelength of the nanoparticles after each coating. (c) Hydrodynamic diameter and (d) zeta potential of the nanoparticles after the addition of each layer. The data shown are the averages of three independent experiments performed in triplicates. The legend in part c also applies to part d.

(+ 47.4 mV) after coating with the first layer of PLL due to the presence of primary amines on the construct surface after coating. Further coating with miR-34a reversed the zeta potential to -2.0 mV, confirming the presence of miR-34a on the surface, and after coating with the last layer of PLL the final charge of the LbL-NS was positive ($+ 53 \pm 5$ mV). It was important that the final zeta potential of the particles be positive to facilitate their efficient entry into cells across the negative lipid bilayer.¹³ Notably, the size and zeta potential measurements were consistent between LbL-NS prepared with miR-34a or miR-co (Figs. 1c and 1d). In addition to directly measuring the size and zeta potential of the NS after addition of each layer, we also analyzed the supernatants of the purified nanoparticles by DLS and zeta potential measurements to qualitatively observe unreacted PLL or miRNA in solution (Table S1). The unreacted PLL and miRNA in the supernatants were also quantified using TNBS and OliGreen assays, respectively, so that we could determine the amount of PLL and miRNA loaded onto the nanoparticles. The TNBS assay showed 4.7×10^{-9} μg of PLL per NS (i.e., NS at an OD of 1 contain

$13 \mu\text{g mL}^{-1}$ PLL) and the OliGreen showed 86% loading of miRNA into LbL-NS.

miR-34a Release from LbL-NS in Phosphate Buffered Saline

The release of miR-34a from LbL-NS stored in $1 \times$ PBS at 37°C was observed over a 5-day period. A negligible amount of miR-34a released before 1 h, as detected by OliGreen assay (Fig. 3). At 2 h, 4% of the cargo was released, which increased to 11% in 24 h. At the end of 120 h, 28% release was observed (Fig. 3a). This cumulative release was calculated by dividing the total amount of miRNA released by the initial amount of miRNA added to the LbL-NS (i.e., LbL-NS released 70 nM of their initial 250 nM cargo over 5 days). We did not extend the observation of release beyond 5 days because the nanoparticles were not exposed to cells for longer than this in our *in vitro* experiments.

We similarly assessed the release of miR-34a from LbL-NS under storage conditions (4°C in 10 mM NaCl) by OliGreen assay and observed no quantifiable

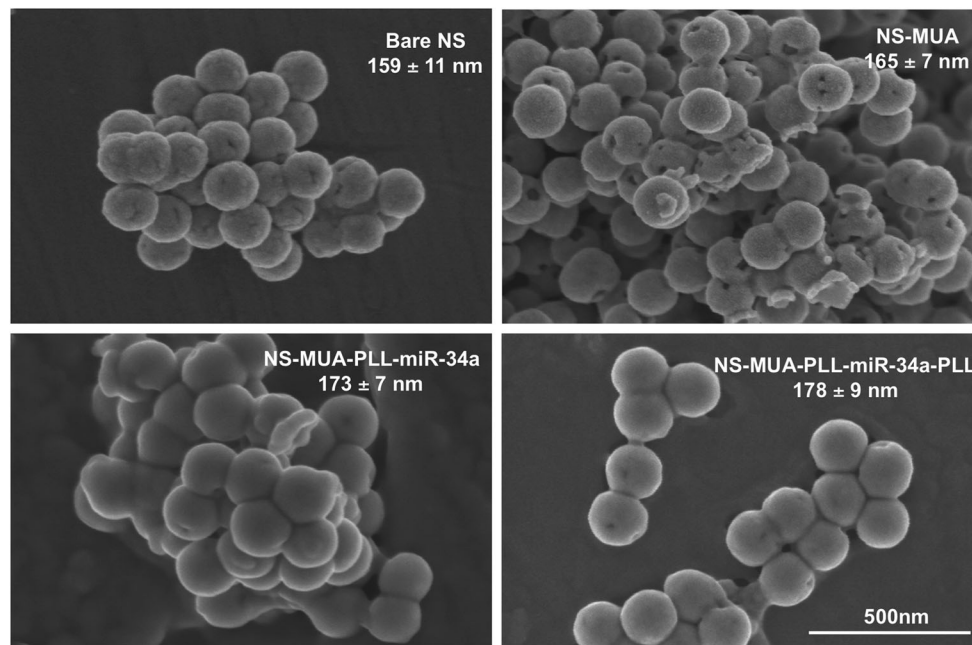


FIGURE 2. Scanning electron micrographs of nanoshells after each coating. The images shown are representative of three independent experiments performed in triplicates, and the data provided are averages and standard deviations of particle diameter measured in ImageJ software. The 500 nm scale bar applies to each image.

release of miR-34a over 66 days. To corroborate this finding, we measured the hydrodynamic diameter and zeta potential of the LbL-NS under storage conditions, and these metrics were also consistent over the 66-day period of study (Fig. S1), indicating the particles are stable under storage conditions.

LbL-NS Enter MDA-MB-231 Cells

To assess the intracellular fate of LbL-NS, live cell confocal microscopy was used to visualize LbL-NS that had been dual-labeled with TRITC-PLL and Cy5-RNA. The intracellular distribution of LbL-NS was compared to that of PLL-RNA polyplexes. Further, because nanomaterials typically undergo endocytosis and ultimately accumulate within lysosomes, lysosomes were visualized using a LAMP1-mGFP fusion protein stably expressed in MDA-MB-231 cells. Following 24 h incubation with cells, both LbL-NS and PLL-RNA polyplexes are clearly visible within cells and appear to accumulate in the perinuclear region (Fig. 4a), characteristic of cargo localized to endocytic compartments. Nanoparticle stability was assessed by determining the extent of signal overlap between the TRITC-PLL and Cy5-RNA. Both constructs appear relatively stable in the intracellular environment, as all MCCs calculated for TRITC-PLL and Cy5-RNA ex-

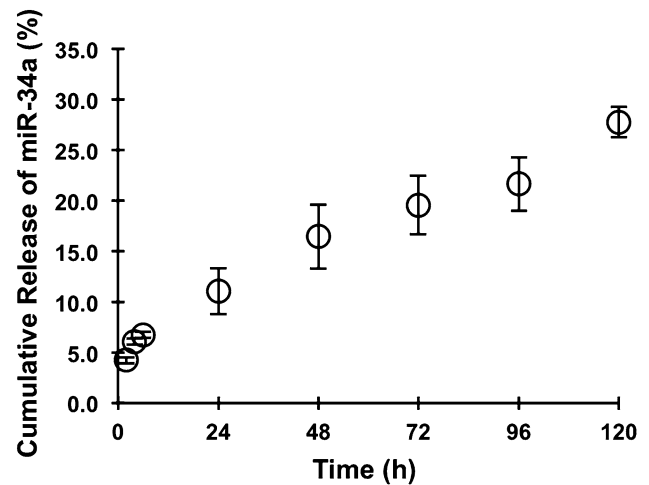


FIGURE 3. Percent cumulative release of miR-34a from LbL-NS at 37 °C in 1× PBS over 120 h.

ceed 0.75 (Fig. 4b, MCC = 0 indicates no colocalization, MCC = 1 indicates perfect colocalization). PLL-RNA polyplexes exhibit a slightly greater tendency to dissociate within cells relative to LbL-NS, as supported by a ~ 10% decrease in MCC calculated for both Cy5-RNA overlapping TRITC-PLL and TRITC-PLL overlapping Cy5-RNA (Fig. 4b). Further, both LbL-NS and PLL-RNA polyplexes appear to traffic to

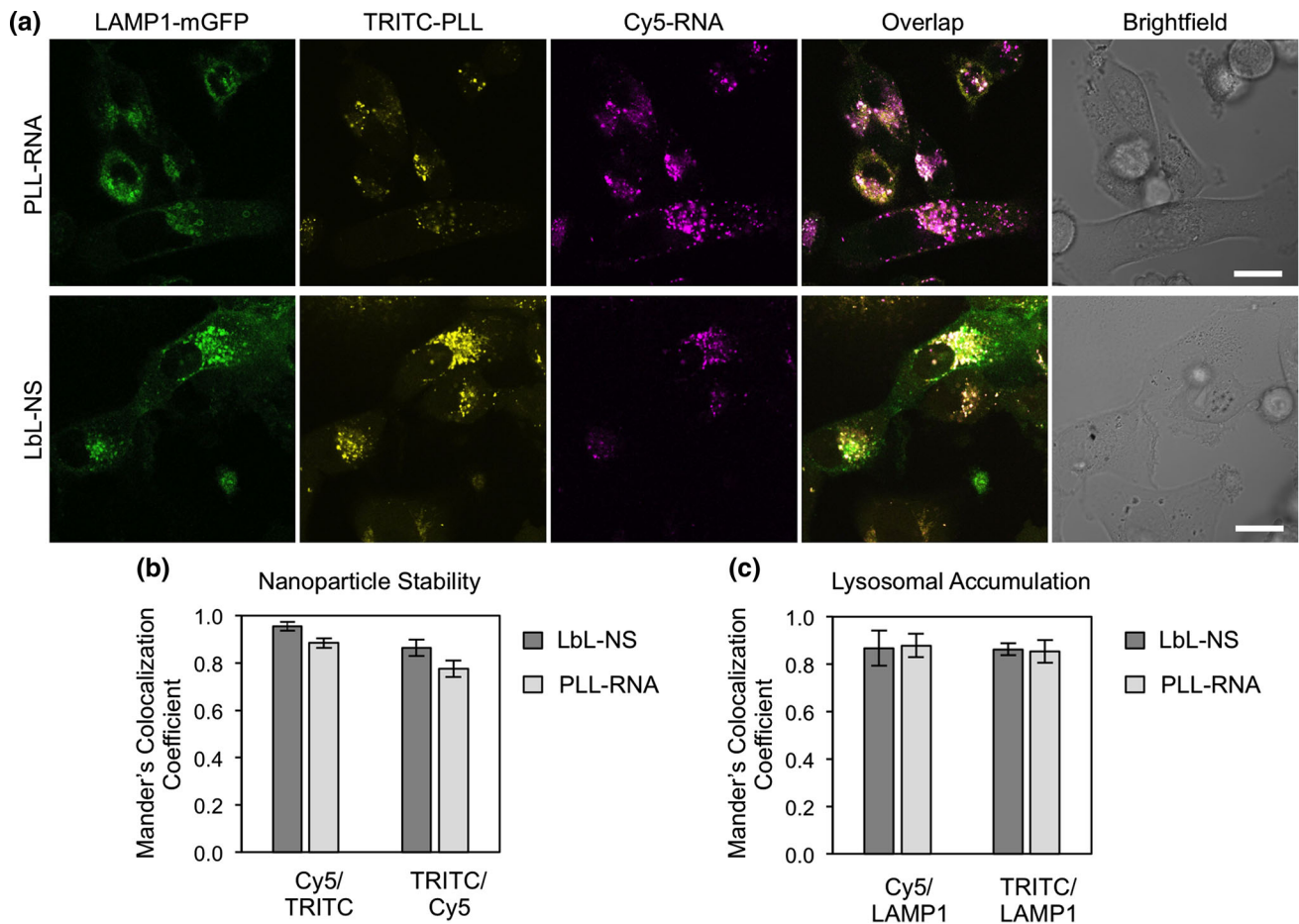


FIGURE 4. (a) Representative confocal microscopy images showing the intracellular fate of LbL-NS or PLL-RNA polyplexes that are dual-labeled with TRITC-PLL and Cy5-RNA. Lysosomes are visualized using MDA-MB-231 cells stably expressing a LAMP1-mGFP fusion protein. Scale bar = 20 μm . (b) MCC's representing the fractional overlap of Cy5-RNA signal with TRITC-PLL and TRITC-PLL overlapping Cy5-RNA, indicating nanoparticle stability. (c) MCC's representing the fractional overlap of Cy5-RNA and TRITC-PLL with LAMP1-mGFP, indicating lysosomal accumulation.

lysosomes, with both particle types appearing highly colocalized with LAMP1-mGFP (all MCCs ~ 0.87 , Fig. 4c). This finding is consistent with literature demonstrating that the fraction of nanoparticle-based nucleic acid carriers that avoid retention within the endolysosomal system is low.^{12,38}

We also analyzed the intracellular distribution of LbL-NS after 72 h incubation, and the results indicate that the majority of the nanoparticles remain colocalized with LAMP1-mGFP-labeled lysosomes at this time point (Fig. S2). This agrees with literature precedent that demonstrates the cytosolic delivery of RNA carriers occurs from maturing endosomes within minutes to a few hours of endocytosis, and that any material in lysosomes after this will remain.^{12,38} We next aimed to evaluate whether the $\sim 13\%$ cytosolic delivery achieved with LbL-NS is sufficient to suppress

expression of the desired miR-34a target genes, SIRT1 and Bcl-2.

LbL-NS Suppress SIRT1 and Bcl-2 Expression

To confirm that the level of cytosolic delivery achieved by LbL-NS in MDA-MB-231 cells is sufficient for gene regulation, we investigated whether cells treated with LbL-NS exhibit reduced expression of Bcl-2 and SIRT1, which are known downstream targets of miR-34a.²⁴ We transfected MDA-MB-231 cells with miR-34a-LbL-NS or miR-co-LbL-NS at equivalent doses and then examined Bcl-2 and SIRT1 protein expression levels using Western blotting. This analysis revealed that miR-34a-LbL-NS significantly decreased Bcl-2 ($35 \pm 3\%$) and SIRT1 ($46 \pm 3\%$) protein levels in MDA-MB-231 cells when compared to controls

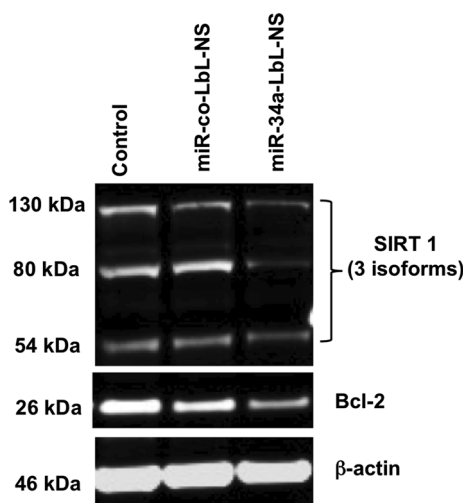


FIGURE 5. Western blot comparing SIRT1 and Bcl-2 expression in MDA-MB-231 cells 72 h after incubation with either miR-co-LbL-NS or miR-34a-LbL-NS.

(Fig. 5). These results show that LbL-NS can efficiently deliver miR-34a to TNBC cells to regulate target gene expression. Next, we aimed to evaluate the nanoparticles' safety, as well as the functional effect of the miR-34a, through analysis of their impact on cellular metabolic activity.

Effect of LbL-NS on MDA-MB-231 Cell Metabolic Activity

We assessed cellular metabolic activity in the presence of free PLL, miR-co-LbL-NS, and miR-34a-LbL-NS in order to reveal the inherent cytocompatibility of the platform and also to begin to distinguish the effect that miR-34a delivered *via* LbL-NS has on cellular function. Metabolic activity was assessed using Alamar Blue assay in cells treated in triplicate with free PLL (1 to 100 $\mu\text{g mL}^{-1}$) or with LbL-NS (0.5–4.0 OD). An increase in OD of NS corresponds to a proportional increase in concentration of miR-34a or miR-co delivered to cells, as well as an increase in the concentration of PLL delivered to cells. Cells exposed to no treatment were considered as 100% viable.

The results show that free PLL did not exhibit any cellular toxicity up to 20 $\mu\text{g mL}^{-1}$ and the cells were $\sim 100\%$ viable (Fig. 6a). Starting at 40 $\mu\text{g mL}^{-1}$ free PLL, the cells were only $\sim 20\%$ viable as compared to control. We have previously shown that NS coated with PEG are non-toxic in MDA-MB-231 cells up to an optical density of 10.³² Here, we found that MDA-MB-231 cells exhibit $> 90\%$ viability when treated with LbL-NS at an OD of 0.5 (Fig. 6b). When the OD of miR-co-LbL-NS was increased to 3, the cells' metabolic activity decreased to $\sim 70\%$, and it was $\sim 65\%$ at OD 4. An OD of 3 corresponds to \sim

40 $\mu\text{g mL}^{-1}$ PLL delivered with LbL-NS and an OD of 4 corresponds to $\sim 50 \mu\text{g mL}^{-1}$ PLL delivered with LbL-NS. This shows that the LbL-NS are more cyto-compatible than free PLL, as cells exposed to 40 $\mu\text{g mL}^{-1}$ free PLL are only 21% viable compared to 70% for LbL-NS, and cells exposed to 50 $\mu\text{g mL}^{-1}$ PLL are only 18% viable compared to 65% for LbL-NS (Fig. S3a). This finding suggests that the nanoscale presentation of PLL to cells is an important feature that dictates its safety.

Notably, by comparing the metabolic activity of cells treated with miR-34a-LbL-NS with that of cells treated with miR-co-LbL-NS, we could begin to probe the functional effects of the delivered miR-34a. At an OD of 3, MDA-MB-231 cells exposed to miR-co-LbL-NS displayed 70% metabolic activity, compared to 50% for miR-34a-LbL-NS, meaning the delivered miR-34a reduced metabolic activity by 29% ($p < 0.05$) (Fig. 6b). Consistently, MDA-MB-231 cells treated with OD4 miR-34a-LbL-NS were 40% viable, which means the delivered miR-34a reduced metabolic activity by 38% relative to miR-co delivered with LbL-NS ($p < 0.05$) (Fig. 6b). The LbL-NS used in this study were made by adding 250 nM miRNA to OD4 PLL-coated NS; the corresponding amount of miRNA for each OD of particles tested are provided for reference in Fig. 6b. Importantly, the metabolic activity of non-cancerous MCF10A cells was unaltered upon treatment with miR-co-LbL-NS or miR-34a-LbL-NS at a dose of OD3 (corresponding to an miRNA dose of ~ 200 nM) (Fig. S3b). These data suggest that LbL-NS can deliver functional miR-34a sufficient to reduce metabolic activity into MDA-MB-231 cells, while minimizing effects on non-cancerous cells. To more directly probe the functionality of the delivered miR-34a in MDA-MB-231 cells, and confirm the safety of LbL-NS in non-cancerous MCF10A cells, we next investigated the impact of LbL-NS and polyplexes on proliferation of each of these cell types, as miR-34a is known to directly regulate proliferation.

LbL-NS Delivering miR-34a Inhibit TNBC Cell Proliferation

The proliferation of MDA-MB-231 cells exposed to LbL-NS or polyplexes prepared with 250 nM of either miR-34a or miR-co was measured with an EdU-based cell proliferation assay at 48 h, where the total incubation time with the various agents was 6 h (Fig. 7). Untreated cells were $89 \pm 4\%$ proliferative at the time point studied, and the cells in all of the control groups (miR-34a or miR-co polyplexes; miR-co-LbL-NS) displayed similar values of 83–87% proliferation (Fig. 7). In contrast, MDA-MB-231 cells treated with miR-34a-LbL-NS showed a significant reduction in

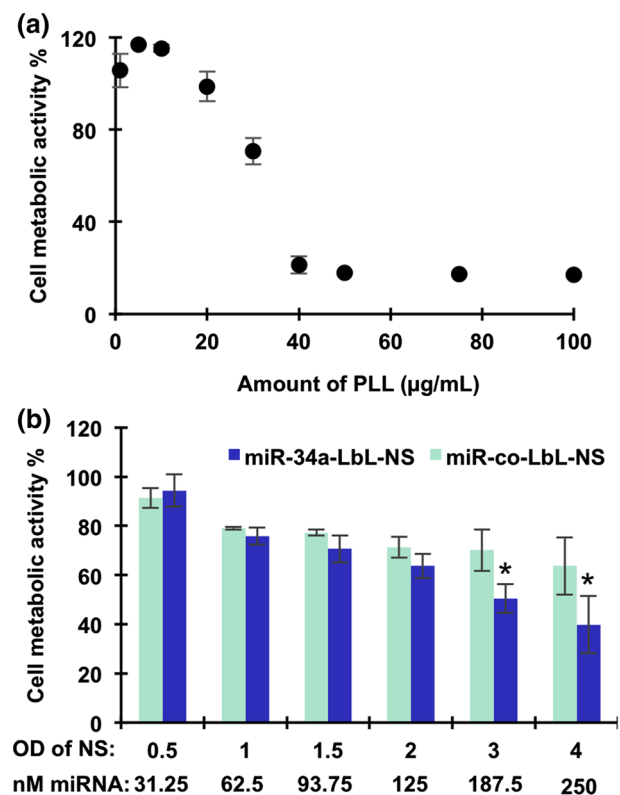


FIGURE 6. Metabolic activity of MDA-MB-231 cells treated with (a) PLL or with (b) miR-34a-LbL-NS or miR-co-LbL-NS, 72 h post-treatment as determined by Alamar Blue assay. * $p < 0.05$ using Student's t test.

proliferation. These cells were $67 \pm 4\%$ proliferating, which is 20% lower than cells exposed to miR-co-LbL-NS ($p < 0.05$) and 21% lower than cells exposed to miR-34a-PLL polyplexes ($p < 0.05$). This data supports the ability of LbL-NS to deliver miR-34a into TNBC cells at levels suitable for altering cellular behavior. Further, it shows that nanoscale architecture plays a critical role in gene regulation potency, as polyplexes that lack controlled architecture did not inhibit cell proliferation, whereas LbL-NS with well-defined architecture had a substantial impact on cell proliferation. Importantly, LbL-NS carrying miR-34a did not reduce the proliferation of non-cancerous MCF10A cells (Fig. S4; these samples were 84% proliferative, as compared to 81–89% for MCF10A cells treated with miR-co-LbL-NS, miR-co-polyplexes, or miR-34a-polyplexes). This demonstrates that miR-34a-LbL-NS can reduce proliferation of TNBC cells while minimizing impact to healthy breast cells.

DISCUSSION

This work demonstrates that layer-by-layer assembled nanoparticles consisting of nanoshells coated with

alternating layers of PLL, miR-34a, and PLL can facilitate the intracellular delivery of miR-34a with more potency and less toxicity than randomly assembled miR-34a-PLL polyplexes. This finding provides critical insight to design considerations for engineering miRNA nanocarriers, and suggests that researchers may be able to capitalize on and manipulate nanoscale architecture to improve miRNA delivery.

To date, various types of nanocarriers have been explored for intracellular miRNA delivery, but only a single agent has progressed into clinical trials. It consisted of a liposomal formulation of miR-34a, but the clinical trial was ended after several patients experienced adverse events.⁵ It could not be concluded whether the adverse events were due to the miR-34a or the liposomal carrier, and this demonstrates the need for additional studies to develop new nanocarriers and elucidate structure/function relationships that will maximize success of miRNA replacement therapies. Among the various materials available as miRNA delivery vehicles, polycationic agents such as PLL are of great interest because they can complex with negatively charged nucleic acids and promote their entry into cells. However, PLL alone is inherently toxic due to the presence of primary amines in its backbone. Here, we hypothesized that changing the presentation of PLL to target cells may enhance miRNA delivery while minimizing cytotoxicity, and we synthesized LbL-NS with controlled PLL and miRNA architecture to evaluate this hypothesis.

To test if nanocarrier architecture can impact polycation-mediated miRNA delivery, we investigated the cellular uptake, cytocompatibility, and gene regulation potency of LbL-NS vs. PLL-miRNA polyplexes. We found that LbL-NS display similar uptake and intracellular localization to PLL-miRNA polyplexes, with ~13% of the nanoparticles escaping lysosomes at 24 h post-delivery. We did not observe any noticeable increase in cytosolic delivery at 72 h, which is consistent with literature reports that demonstrate cytosolic delivery of RNA carriers occurs from maturing endosomes within minutes to a few hours of endocytosis.^{12,38} We believe the achieved 13% cytosolic delivery is biologically impactful given that studies have shown endosome escape is an inefficient process, with just 1–2% of nucleic acid cargo typically reaching the cytosol.¹² Importantly, less than a few thousand copies of RNA are required in the cytosol to achieve gene silencing,³⁸ and the amount of miRNA delivered to the cytosol with LbL-NS is above this threshold.

We also demonstrated that LbL-NS are more cytocompatible than free PLL, and that they are more potent at inhibiting TNBC cell proliferation than randomly assembled PLL-miR-34a polyplexes. We attribute this improved cytocompatibility and potency

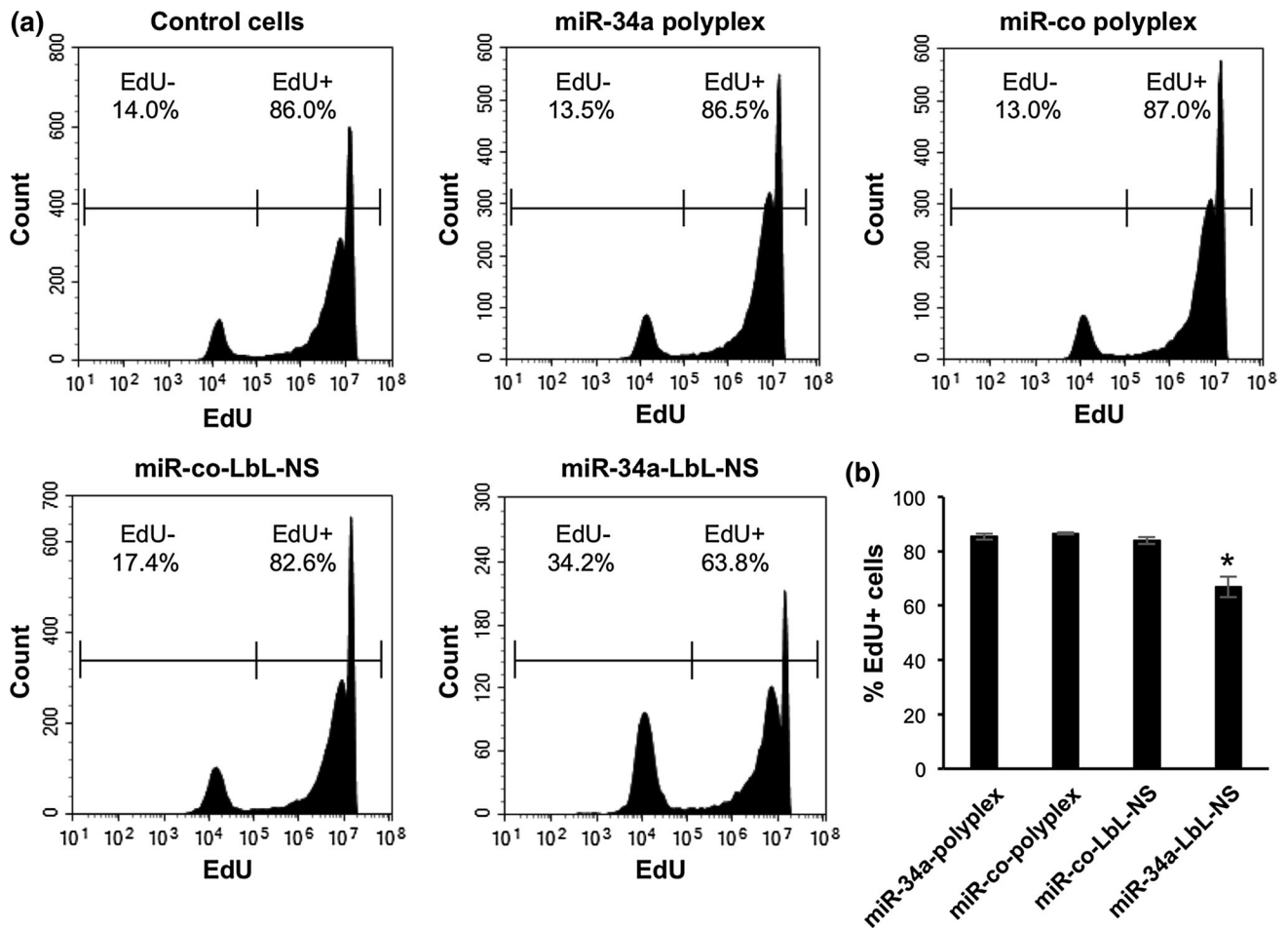


FIGURE 7. Flow cytometry analysis of MDA-MB-231 cell proliferation 72 h after treatment with polyplexes or LbL-NS carrying miR-34a or miR-co. The data in (a) are representative of three independent experiments run in triplicate, and the data in (b) are the average and standard deviation of the triplicate experiments. * $p < 0.05$ compared to all other groups by ANOVA.

to the altered presentation of PLL and miR-34a in the LbL-NS system. While LbL-NS contain a core nano-shell particle that polyplexes do not contain, we do not believe the core influences the cellular interactions of the platform because layer-by-layer assembled nanoparticles based on other core materials (such as poly(lactic-co-glycolic acid) (PLGA), polystyrene, quantum dots, liposomes, and solid gold) have also been shown to be effective for gene regulation without inducing toxicity.^{9,11,16,31}

Finally, we also found that LbL-NS can functionally impair TNBC cells without negatively impacting non-cancerous MCF10A breast epithelial cells. We attribute this specificity to the fact that MCF10A cells have substantially higher inherent expression of miR-34a than MDA-MB-231 cells.² Since miR-34a is already maximally expressed in MCF10A cells, the introduction of more miR-34a *via* LbL-NS has no impact on these cells. Conversely, since MDA-MB-231

cells have almost complete loss of miR-34a expression,² its reintroduction *via* LbL-NS has a profound impact on their viability and proliferation.

Overall, our findings lead us to conclude that the nanoscale presentation of PLL and miRNA to cells is important in dictating both safety and therapeutic efficacy. Layer-by-layer assembled nanoparticles with well-defined architecture offer substantial improvements compared to polyplexes that lack controlled architecture, and our findings warrant continued investigation into structure/function relationships of miRNA nanocarriers.

CONCLUSIONS

We have successfully demonstrated the LbL assembly of the oppositely charged polyelectrolytes miR-34a and PLL on the surface of NS and shown

that the resultant LbL-NS are effective vehicles for intracellular miRNA delivery. The use of layer-by-layer synthesis offers a unique strategy to fabricate well defined and homogeneously distributed miRNA nanocarriers, which we demonstrate are more effective than polyplexes with uncontrolled architecture. Indeed, cellular trafficking experiments revealed that LbL-NS are internalized by endocytosis, and display similar intracellular localization to polyplexes. The downregulation of SIRT1 and Bcl-2, two known targets of miR-34a, in MDA-MB-231 cells by LbL-NS suggests that the particles can sufficiently deliver miRNA into these cells. This is supported by the fact that cells treated with miR-34a-LbL-NS display reduced metabolic activity and proliferation relative to cells exposed to controls. Together, these findings warrant further study of LbL-NS as miRNA delivery vehicles for RNAi therapy of various diseases. The information engendered by these studies would be useful to unravel the path towards designing new nanomaterials for miRNA replacement therapy.

ELECTRONIC SUPPLEMENTARY MATERIAL

The online version of this article (<https://doi.org/10.1007/s12195-018-0535-x>) contains supplementary material, which is available to authorized users.

ACKNOWLEDGMENTS

This work was supported by the National Institute of General Medical Sciences of the National Institutes of Health (NIH) under Award Number R35GM119659 (PI:Day). JRM received support from the Department of Defense through a National Defense Science and Engineering Graduate Fellowship. The content is solely the responsibility of the authors and does not necessarily represent the views of the funding agencies. The LSM880 confocal microscope was acquired with a shared instrumentation Grant (S10 OD016361) and access was supported by the NIH-NIGMS (P20 GM103446), the NSF (IIA-1301765), and the State of Delaware. The Hitachi S4700 used in this work was acquired with the Delaware INBRE Grant P20 GM103446.

AUTHOR CONTRIBUTIONS

All authors conceptualized the experiments. RG, CK, JM, and RR performed the experiments and analyzed the data. ED secured funding for the experiments. All authors wrote and revised the manuscript.

CONFLICT OF INTEREST

Ritu Goyal, Chintan Kapadia, Jilian Melamed, Rachel Riley, and Emily Day declare no conflicts of interest.

ETHICAL STANDARDS

No animal or human studies were performed in this work.

REFERENCES

- ¹Adams, B. D., C. Parsons, and F. J. Slack. The tumor-suppressive and potential therapeutic functions of miR-34a in epithelial carcinomas. *Expert Opin. Ther. Targets* 20(6):737–753, 2016.
- ²Adams, B., V. Wali, C. Cheng, S. Inukai, C. Booth, S. Agarwal, D. Rimm, B. Györfy, L. Santarpia, L. Pusztai, W. Saltzman, and F. Slack. miR-34a silences c-SRC to attenuate tumor growth in triple-negative breast cancer. *Cancer Res.* 76(4):927–939, 2016.
- ³Avery-Kiejda, K. A., S. G. Braye, A. Mathe, J. F. Forbes, and R. J. Scott. Decreased expression of key tumor suppressor microRNAs is associated with lymph node metastasis in triple negative breast cancer. *BMC Cancer* 14:51, 2014.
- ⁴Bartel, D. P. MicroRNAs: target recognition and regulatory functions. *Cell* 136(2):215–233, 2009.
- ⁵Beg, M. S., A. J. Brenner, J. Sachdev, M. Borad, Y. K. Kang, J. Stoudemire, S. Smith, A. G. Bader, S. Kim, and D. S. Hong. Phase I study of MEX34, a liposomal mir-34a mimic, administered twice weekly in patients with advanced solid tumors. *Invest New Drugs* 35(2):180–188, 2017.
- ⁶Ben-Shushan, D., E. Markovskiy, H. Gibori, G. Tiram, A. Scomparin, and R. Satchi-Fainaro. Overcoming obstacles in microRNA delivery towards improved cancer therapy. *Drug Deliv. Transl. Res.* 4(1):38–49, 2014.
- ⁷Calin, G. A., and C. M. Croce. MicroRNA signatures in human cancers. *Nat. Rev. Cancer* 6(11):857–866, 2006.
- ⁸Deng, X., M. Cao, J. Zhang, K. Hu, Z. Yin, Z. Zhou, X. Xiao, Y. Yang, W. Sheng, Y. Wu, and Y. Zeng. Hyaluronic acid-chitosan nanoparticles for co-delivery of miR-34a and doxorubicin in therapy against triple negative breast cancer. *Biomaterials* 35(14):4333–4344, 2014.
- ⁹Deng, Z. J., S. W. Morton, E. Ben-Akiva, E. C. Dreaden, K. E. Shopsowitz, and P. T. Hammond. Layer-by-layer nanoparticles for systemic codelivery of an anticancer drug and siRNA for potential triple-negative breast cancer treatment. *ACS Nano* 7(11):9571–9584, 2013.
- ¹⁰Duff, D. G., A. Baiker, and P. P. Edwards. A new hydrosol of gold clusters. 1. Formation and particle-size variation. *Langmuir* 9(9):2301–2309, 1993.
- ¹¹Elbakry, A., A. Zaky, R. Liebl, R. Rachel, A. Goepferich, and M. Breunig. Layer-by-layer assembled gold nanoparticles for siRNA delivery. *Nano Lett.* 9(5):2059–2064, 2009.
- ¹²Gilleron, J., W. Querbes, A. Zeigerer, A. Borodovsky, G. Marsico, U. Schubert, K. Manygoats, S. Seifert, C. Andree, M. Stoter, H. Epstein-Barash, L. Zhang, V. Kotliansky, K. Fitzgerald, E. Fava, M. Bickle, Y. Kalaidzidis, A.

- Akinc, M. Maier, and M. Zerial. Image-based analysis of lipid nanoparticle-mediated siRNA delivery, intracellular trafficking and endosomal escape. *Nat Biotechnol.* 31(7):638–646, 2013.
- ¹³Goyal, R., S. K. Tripathi, S. Tyagi, A. Sharma, K. R. Ram, D. K. Chowdhuri, Y. Shukla, P. Kumar, and K. C. Gupta. Linear PEI nanoparticles: efficient pDNA/siRNA carriers in vitro and in vivo. *Nanomedicine* 8(2):167–175, 2012.
- ¹⁴Goyal, R., S. K. Tripathi, E. Vazquez, P. Kumar, and K. C. Gupta. Biodegradable poly(vinyl alcohol)-polyethylenimine nanocomposites for enhanced gene expression in vitro and in vivo. *Biomacromolecules* 13(1):73–83, 2012.
- ¹⁵Grotzky, A., Y. Manaka, S. Fornera, M. Willeke, and P. Walde. Quantification of alpha-polylysine: a comparison of four UV/Vis spectrophotometric methods. *Anal. Methods* 2(10):1448–1455, 2010.
- ¹⁶Gu, L., Z. J. Deng, S. Roy, and P. T. Hammond. A combination RNAi-chemotherapy layer-by-layer nanoparticle for systemic targeting of KRAS/p53 with cisplatin to treat non-small cell lung cancer. *Clin. Cancer Res.* 23(23):7312–7323, 2017.
- ¹⁷Hao, L., P. C. Patel, A. H. Alhasan, D. A. Giljohann, and C. A. Mirkin. Nucleic acid-gold nanoparticle conjugates as mimics of microRNA. *Small* 7(22):3158–3162, 2011.
- ¹⁸Kim, V. N. MicroRNA biogenesis: coordinated cropping and dicing. *Nat. Rev. Mol. Cell Biol.* 6:376–385, 2005.
- ¹⁹Kouri, F. M., L. A. Hurlley, W. L. Daniel, E. S. Day, Y. Hua, L. Hao, C.-Y. Peng, T. J. Merkel, M. A. Queisser, C. Ritner, H. Zhang, C. D. James, J. I. Sznajder, L. Chin, D. A. Giljohann, J. A. Kessler, M. E. Peter, C. A. Mirkin, and A. H. Stegh. miR-182 integrates apoptosis, growth, and differentiation programs in glioblastoma. *Genes Dev.* 29(7):732–745, 2015.
- ²⁰Kreuzberger, N. L., J. R. Melamed, and E. S. Day. Nanoparticle-mediated gene regulation as a novel strategy for cancer therapy. *Del. J. Public Health* 3(3):20–24, 2017.
- ²¹Krzeszinski, J. Y., W. Wei, H. Huynh, Z. Jin, X. Wang, T.-C. Chang, X.-J. Xie, L. He, L. S. Mangala, G. Lopez-Berestein, A. K. Sood, J. T. Mendell, and Y. Wan. miR-34a blocks osteoporosis and bone metastasis by inhibiting osteoclastogenesis and Tgif2. *Nature* 512(7515):431–435, 2014.
- ²²Kuo, W.-H., Y.-Y. Chang, L.-C. Lai, M.-H. Tsai, C. K. Hsiao, K.-J. Chang, and E. Y. Chuang. Molecular characteristics and metastasis predictor genes of triple-negative breast cancer: a clinical study of triple-negative breast carcinomas. *PLOS ONE* 7(9):e45831, 2012.
- ²³Li, L., X. Xie, J. Luo, M. Liu, S. Xi, J. Guo, Y. Kong, M. Wu, J. Gao, Z. Xie, J. Tang, X. Wang, W. Wei, M. Yang, M.-C. Hung, and X. Xie. Targeted expression of mir-34a using the t-visa system suppresses breast cancer growth and invasion. *Mol. Ther.* 20(12):2326–2334, 2012.
- ²⁴Li, L., L. Yuan, J. Luo, J. Gao, J. Guo, and X. Xie. miR-34a inhibits proliferation and migration of breast cancer through down-regulation of Bcl-2 and SIRT1. *Clin. Exp. Med.* 13:109–117, 2013.
- ²⁵Liedtke, C., C. Mazouni, K. R. Hess, F. Andre, A. Tordai, J. A. Mejia, W. F. Symmans, A. M. Gonzalez-Angulo, B. Hennessy, M. Green, M. Cristofanilli, G. N. Hortobagyi, and L. Pusztai. Response to neoadjuvant therapy and long-term survival in patients with triple-negative breast cancer. *J. Clin. Oncol.* 26:1275–1281, 2008.
- ²⁶MacFarlane, L.-A., and P. R. Murphy. MicroRNA: biogenesis, function and role in cancer. *Curr. Genom.* 11(7):537–561, 2010.
- ²⁷Manders, E. M. M., F. J. Verbeek, and J. A. Aten. Measurement of co-localization of objects in dual-colour confocal images. *J. Microsc.* 169(3):375–382, 1993.
- ²⁸Melamed, J., R. Riley, D. Valcourt, M. Billingsley, N. Kreuzberger, and E. Day. Quantification of siRNA duplexes bound to gold nanoparticle surfaces. In: *Biomedical Nanotechnology: Methods and Protocols* 2nd, edited by S. H. Petrosko, and E. S. Day. New York: Humana Press, 2017, pp. 1–15.
- ²⁹Missio, G., M. T. D. Martino, G. D. Rosa, A. A. Farooqi, A. Lombardi, V. Campani, M. R. Zarone, A. Gullà, P. Tagliaferri, P. Tassone, and M. Caraglia. miR-34: a new weapon against cancer? *Molec. Ther. Nucleic Acids* 3:e194, 2014.
- ³⁰Oldenburg, S. J., R. D. Averitt, S. L. Westcott, and N. J. Halas. Nanoengineering of optical resonances. *Chem. Phys. Lett.* 288(2–4):243–247, 1998.
- ³¹Poon, Z., D. Chang, X. Zhao, and P. T. Hammond. Layer-by-layer nanoparticles with a pH-sheddable layer for in vivo targeting of tumor hypoxia. *ACS Nano* 5(6):4284–4292, 2011.
- ³²Riley, R. S., and E. S. Day. Frizzled7 antibody-functionalized nanoshells enable multivalent binding for Wnt signaling inhibition in triple negative breast cancer cells. *Small* 13(26):1700544, 2017.
- ³³Rokavec, M., H. Li, L. Jiang, and H. Hermeking. The p53/miR-34 axis in development and disease. *J. Mol. Cell Biol.* 6(3):214–230, 2014.
- ³⁴Saito, Y., T. Nakaoka, and H. Saito. MicroRNA-34a as a therapeutic agent against human cancer. *J. Clin. Med.* 4(11):1951–1959, 2015.
- ³⁵Sparrow, J. T., V. V. Edwards, C. Tung, M. J. Logan, M. S. Wadhwa, J. Duguid, and L. C. Smith. Synthetic peptide-based DNA complexes for nonviral gene delivery. *Adv. Drug Deliv. Rev.* 30(1–3):115–131, 1998.
- ³⁶Stern, J. M., V. V. Kibanov Solomonov, E. Sazykina, J. A. Schwartz, S. C. Gad, and G. P. Goodrich. Initial evaluation of the safety of nanoshell-directed photothermal therapy in the treatment of prostate disease. *Int. J. Toxicol.* 35(1):38–46, 2016.
- ³⁷Swami, A., R. Goyal, S. K. Tripathi, N. Singh, N. Katiyar, A. K. Mishra, and K. C. Gupta. Effect of homobifunctional crosslinkers on nucleic acids delivery ability of PEI nanoparticles. *Int. J. Pharm.* 374(1–2):125–138, 2009.
- ³⁸Wittrup, A., A. Ai, X. Liu, P. Hamar, R. Trifonova, K. Charisse, M. Manoharan, T. Kirchhausen, and J. Lieberman. Visualizing lipid-formulated siRNA release from endosomes and target gene knockdown. *Nat. Biotechnol.* 33:870–876, 2015.
- ³⁹Wu, Z. W., C. T. Chien, C. Y. Liu, J. Y. Yan, and S. Y. Lin. Recent progress in copolymer-mediated siRNA delivery. *J. Drug Target.* 20(7):551–560, 2012.
- ⁴⁰Yamakuchi, M., M. Ferlito, and C. J. Lowenstein. miR-34a repression of SIRT1 regulates apoptosis. *Proc. Natl. Acad. Sci. USA* 105(36):13421–13426, 2008.